

Coexistence of localized and itinerant electrons in BaFe_2X_3 ($X = \text{S}$ and Se) revealed by photoemission spectroscopy

D. Ootsuki,¹ N. L. Saini,² F. Du,^{3,4} Y. Hirata,³ K. Ohgushi,^{5,3} Y. Ueda,^{6,3} and T. Mizokawa^{7,1,2}

¹Department of Physics, University of Tokyo, Kashiwa, Chiba 277-8561, Japan

²Department of Physics, Università di Roma "La Sapienza", Piazzale Aldo Moro 2, 00185 Roma, Italy

³Institute for Solid State Physics, University of Tokyo, Kashiwa, Chiba 277-8581, Japan

⁴Key Laboratory of Physics and Technology for Advanced Batteries (Ministry of Education), College of Physics, Jilin University, Changchun, 130012, People's Republic of China

⁵Department of Physics, Tohoku University, Sendai, Miyagi 980-8578, Japan

⁶Toyota Physical and Chemical Institute, Nagakute, Aichi 480-1192, Japan

⁷Department of Complexity Science and Engineering, University of Tokyo, 5-1-5 Kashiwanoha, Kashiwa, Chiba 277-8561, Japan

(Dated: January 12, 2015)

We report a photoemission study at room temperature on BaFe_2X_3 ($X = \text{S}$ and Se) and CsFe_2Se_3 in which two-leg ladders are formed by the Fe sites. The Fe $2p$ core-level peaks of BaFe_2X_3 are broad and exhibit two components, indicating that itinerant and localized Fe $3d$ sites coexist similar to $\text{K}_x\text{Fe}_{2-y}\text{Se}_2$. The Fe $2p$ core-level peak of CsFe_2Se_3 is rather sharp and is accompanied by a charge-transfer satellite. The insulating ground state of CsFe_2Se_3 can be viewed as a Fe^{2+} Mott insulator in spite of the formal valence of +2.5. The itinerant versus localized behaviors can be associated with the stability of chalcogen p holes in the two-leg ladder structure.

PACS numbers: 74.25.Jb, 74.70.Xa, 79.60.-i, 74.81.-g

I. INTRODUCTION

The coexistence of itinerant superconducting phase and localized antiferromagnetic phase in $\text{K}_x\text{Fe}_{2-y}\text{Se}_2$ [1–4] sheds light on the intervening coupling between the electron correlation effect and the lattice effect. When the Fe $3d$ electrons are localized and form the antiferromagnetic insulating state with high-spin Fe^{2+} , the insulating phase tends to expand due to Fe-Fe bond length increase and applies a kind of pressure to the remaining metallic region. [5] The antiferromagnetic insulating phase in $\text{K}_x\text{Fe}_{2-y}\text{Se}_2$ is identified as $\text{K}_2\text{Fe}_4\text{Se}_5$ with Fe vacancy order. [2, 3] On the other hand, the superconducting phase is likely to be FeSe which is under the pressure from the expanded and insulating $\text{K}_2\text{Fe}_4\text{Se}_5$. In the insulating $\text{K}_2\text{Fe}_4\text{Se}_5$ phase, the four Fe sites with square geometry form a ferromagnetic block which couples antiferromagnetically with neighboring blocks. [3] The transfer integrals between the neighboring blocks are reduced due to the Fe vacancy, and the Mott insulating state is realized. In the XPS study on $\text{K}_x\text{Fe}_{2-y}\text{Se}_2$, two components of the Fe $2p_{3/2}$ peak are assigned to the coexisting superconducting and insulating phases in the superconducting $\text{K}_x\text{Fe}_{2-y}\text{Se}_2$ while, in insulating $\text{K}_x\text{Fe}_{2-y}\text{Se}_2$, the Fe $2p_{3/2}$ peak consists of a single component. [6] The charge-transfer energy from Se $4p$ to Fe $3d$ is estimated to be 2.3 eV which is smaller than the repulsive Coulomb interaction between the Fe $3d$ electrons of 3.5 eV. [6] Therefore, the insulating $\text{K}_2\text{Fe}_4\text{Se}_5$ phase with high-spin Fe^{2+} can be regarded as a Mott insulating state of charge-transfer type instead of Mott-Hubbard-type, and the Se $4p$ orbitals should be taken into account to explain the magnetic interactions between the Fe spins.

Recently, another insulating Fe selenide BaFe_2Se_3 has

been attracting much attention due to the specific quasi one-dimensional crystal structure with Pnma space group as well as the block-type antiferromagnetic state similar to $\text{K}_2\text{Fe}_4\text{Se}_5$. [7–13] In addition, BaFe_2Se_3 is predicted to be a new type of multiferroic system with magnetic and ferroelectric orders in a recent theoretical work, [14] which certainly enhances the interest in the title system. In BaFe_2Se_3 , FeSe_4 tetrahedra share their edges and form a two-leg ladder of Fe sites as shown in Fig. 1(a). The magnetic structure of BaFe_2Se_3 is similar to $\text{K}_2\text{Fe}_4\text{Se}_5$ in that four Fe spins in the two-leg ladder form a ferromagnetic block and the neighboring blocks are antiferromagnetically coupled as illustrated in Fig. 1. The two-leg ladder is distorted with shorter Fe-Fe bonds (ferromagnetic and antiferromagnetic) and longer Fe-Fe bonds (ferromagnetic and antiferromagnetic) along the ladder direction. The magnetic structure is consistent with the theoretical prediction. [15] Néel temperature reported in the literatures varies from 240 K [9] to 255 K. [7, 8, 11] Also the magnetic moment of BaFe_2Se_3 ranges from $2.1 \mu_B$ [9] to $2.8 \mu_B$ [7, 11] depending on the growth condition, and is smaller than the value expected for high-spin Fe^{2+} . Interestingly, resistivity also depends on the growth condition. Lei *et al.* reported that resistivity exhibits activation-type temperature dependence with band gap of 0.18 eV. [8] On the other hand, one-dimensional variable range hopping was reported by Nambu *et al.* indicating that some carriers are localized due to strong scattering effect in the quasi one-dimensional structure. [11] In addition, coexistence of itinerant and localized electrons was recently indicated by the resonant inelastic x-ray scattering study by Monney *et al.* [12] This observation suggests that the itinerant electrons introduced by small Fe vacancy or some other effects would be responsible for

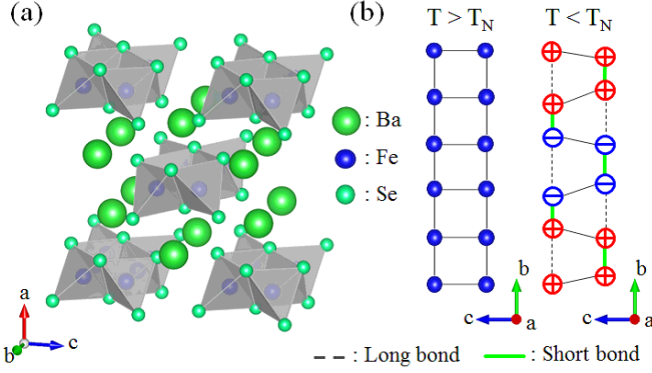


FIG. 1: (Color online) (a) Crystal structure of BaFe_2Se_3 visualized using the software package Vesta[18]. (b) Schematic drawing for the magnetic structure and the lattice distortion for BaFe_2Se_3 .

the reduction of the magnetic moment and the variable range hopping behavior of the resistivity. [11] In contrast to BaFe_2Se_3 , CsFe_2Se_3 with formal Fe valence of +2.5 is much more insulating. [16] Interestingly, Fei *et al.* have revealed that all the Fe sites have the same local environment in CsFe_2Se_3 by means of Mössbauer spectroscopy. [16] Below 177 K, Fe spins in the two-leg ladder of CsFe_2Se_3 order antiferromagnetically along the rung and ferromagnetically along the leg with magnetic moment of $\sim 1.8 \mu_B$. Usually, Mott insulators with integer number of valence are expected to be more insulating than the mixed valence systems. The situation of the two-leg ladder Fe chalcogenides is opposite to this expectation, and CsFe_2Se_3 with formal Fe valence of +2.5 is more insulating than integer valence BaFe_2Se_3 and BaFe_2S_3 . [16] Such puzzling mismatch between the formal valence and the transport behavior indicates unusual electronic states of the title system.

In the present work, we study fundamental electronic structures of BaFe_2Se_3 , BaFe_2S_3 , and CsFe_2Se_3 above their Néel temperatures by means of x-ray photoemission spectroscopy (XPS) and ultra-violet photoemission spectroscopy (UPS) at room temperature. The broad Fe 2*p* XPS peaks of BaFe_2Se_3 and BaFe_2S_3 indicate coexistence of localized and itinerant electrons. On the other hand, the Fe 2*p* XPS peak of CsFe_2Se_3 is relatively sharp suggesting that Fe valence is homogeneous in spite of the expectation of a mixed valence state. The apparent contradiction between the valence state and the Fe 2*p* peak width can be reconciled by taking account of the Se 4*p* or S 3*p* holes.

II. EXPERIMENTS

The single crystals of BaFe_2Se_3 , BaFe_2S_3 , and CsFe_2Se_3 were grown as reported in the literatures. [11, 16] We cleaved the single crystals at room temperature (300 K) under the ultrahigh vacuum for the XPS and

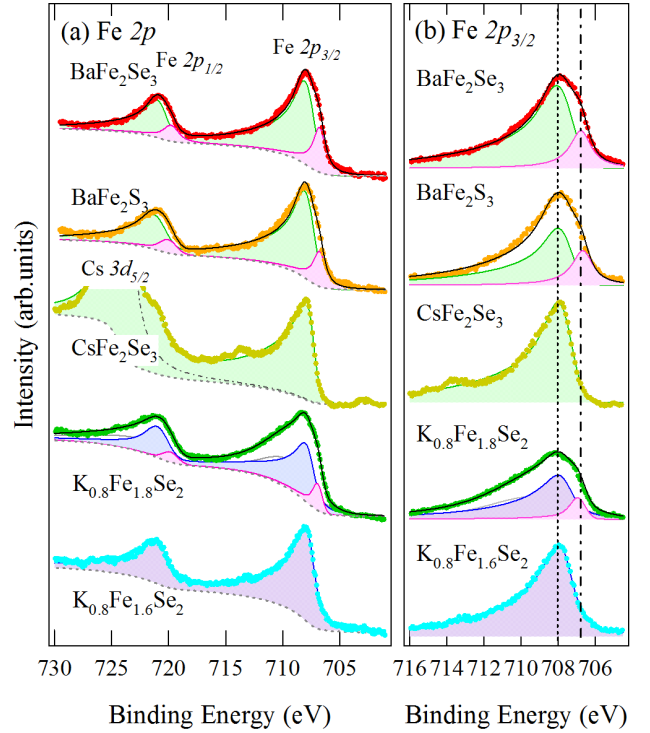


FIG. 2: (Color online) Fe 2*p* XPS of BaFe_2X_3 ($X = \text{S}$ and Se) compared with CsFe_2Se_3 and $\text{K}_x\text{Fe}_{2-y}\text{Se}_2$ (metallic and insulating). [6] The solid curves indicate the results of curve fitting for BaFe_2S_3 and BaFe_2Se_3 .

UPS measurements. The XPS measurement was carried out at 300 K using JPS9200 analyzer. $\text{Mg K}\alpha$ (1253.6 eV) was used as an x-ray source. The total energy resolution was set to ~ 1.0 eV. The binding energy was calibrated using the Au 4*f* core level of the gold reference sample. The UPS measurement was performed using SES100 analyzer and a He I (21.2 eV) source. The total energy resolution was set to ~ 30 meV and the Fermi level was determined using the Fermi edge of the gold reference sample.

III. RESULTS AND DISCUSSION

Figure 2 shows the Fe 2*p* XPS spectra of BaFe_2Se_3 , BaFe_2S_3 , and CsFe_2Se_3 taken at 300 K which are compared with those of superconducting and non-superconducting $\text{K}_x\text{Fe}_{2-y}\text{Se}_2$. [6] In non-superconducting $\text{K}_x\text{Fe}_{2-y}\text{Se}_2$, the chemical composition is close to $\text{K}_2\text{Fe}_4\text{Se}_5$ with Fe^{2+} and its ground state is a charge-transfer-type Mott insulator. The sharp Fe 2*p* peak of CsFe_2Se_3 is very similar to that of non-superconducting $\text{K}_x\text{Fe}_{2-y}\text{Se}_2$ or the Fe^{2+} Mott insulator. This XPS result indicates that CsFe_2Se_3 would be a Mott insulator with Fe^{2+} which is actually consistent with the Mössbauer study. [16] If all the Fe sites in CsFe_2Se_3 take the high-spin Fe^{2+} configuration, the extra positive

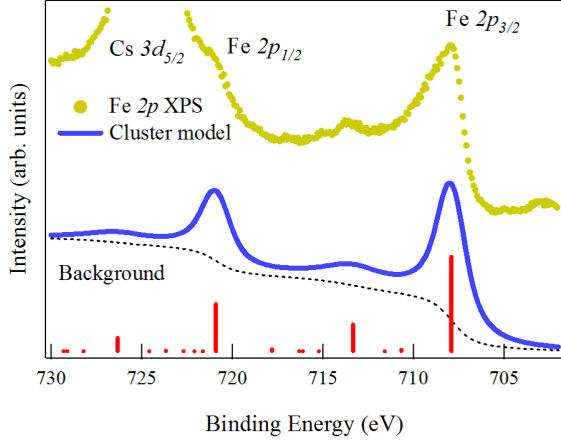


FIG. 3: (Color online) Fe 2p XPS of CsFe₂Se₃ (dots) compared with the result of cluster model calculation. The dotted curve indicates the background due to the secondary electrons.

charge (+0.5 per Fe) should be located at the Se sites. On the other hand, in superconducting K_xFe_{2-y}Se₂, itinerant Fe 3d electrons coexist with the localized Fe 3d electrons in the Mott insulating phase. The Fe 2p line-shape of BaFe₂Se₃ and BaFe₂S₃ is very similar to that of superconducting K_xFe_{2-y}Se₂, indicating coexistence of itinerant and localized electrons. In case of superconducting K_xFe_{2-y}Se₂, the coexistence of the localized and itinerant electronic states is governed by the spatial distribution of the Fe vacancy. On the other hand, BaFe₂Se₃ and BaFe₂S₃ have no Fe vacancy which can reduce transfer integrals between neighboring Fe sites and cause the Mott localization. Instead, in the two-leg ladder structure of BaFe₂Se₃ and BaFe₂S₃, the electronic interaction between neighboring Fe sites can be controlled by the Se 4p or S 3p holes which are indicated by the mismatch between the formal valence and the transport behavior. Here, one can speculate that the Fe 3d electrons with the Fe²⁺ high-spin configuration and the Se 4p (or S 3p) holes are localized in CsFe₂Se₃ whereas they are partially delocalized in BaFe₂Se₃ and BaFe₂S₃.

The Fe 2p_{3/2} and Fe 2p_{1/2} peaks can be decomposed into the two components which are derived from the itinerant and localized parts. In Fig. 2, the results of Mahan's line shape fitting are indicated by the solid curves for BaFe₂Se₃ and BaFe₂S₃. The itinerant component has lower binding energy due to the stronger screening effect. The intensity ratio between the itinerant and localized components is 3.0 : 5.0 for BaFe₂Se₃ and 2.3 : 5.0 for BaFe₂S₃, respectively. The relative intensity of the "itinerant" component is much larger in BaFe₂Se₃ and BaFe₂S₃ than that in K_xFe_{2-y}Se₂. The energy splitting between the two components is ~ 0.8 eV for BaFe₂Se₃ and BaFe₂S₃ which is comparable to the value for K_xFe_{2-y}Se₂.

Figure 3 shows the Fe 2p XPS of CsFe₂Se₃ compared

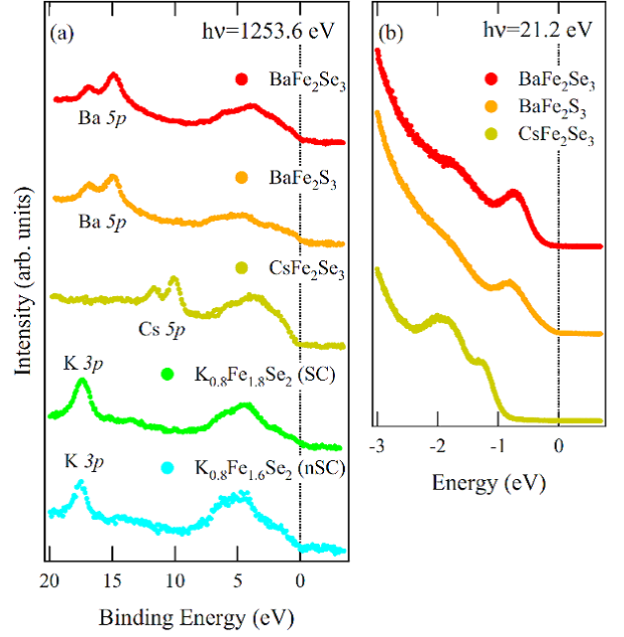


FIG. 4: (Color online) (a) Valence-band XPS of BaFe₂X₃ (X = S and Se) compared with CsFe₂Se₃ and K_xFe_{2-y}Se₂ (metallic and insulating). [6] (b) UPS of BaFe₂X₃ (X = S and Se) compared with CsFe₂Se₃.

with the result of the configuration interaction calculation on an FeSe₄ cluster model. The Fe 2p_{3/2} peak of CsFe₂Se₃ (located around 708 eV) is accompanied by a broad satellite structure (located around 714 eV) which can be assigned to the charge-transfer satellite. The energy position and the intensity of the charge-transfer satellite can be analyzed using the configuration-interaction calculation on the tetrahedral FeSe₄ cluster model. [6] The ground state is assumed to take the high-spin d^6 state mixed with the d^7L , d^8L^2 , d^9L^3 , and $d^{10}L^4$ states where L represents a hole in the Se 4p ligand orbitals. The excitation energy from d^6 to d^7L corresponds to the charge-transfer energy Δ . The excitation energy from d^7L to d^8L^2 is given by $\Delta + U$ where U represents the Coulomb interaction between the Fe 3d electrons. The transfer integrals between the d^nL^m and $d^{n+1}L^{m+1}$ are described by $(pd\sigma)$ and $(pd\pi)$, where the ratio $(pd\sigma)/(pd\pi)$ is fixed at -2.16. The final states are spanned by the cd^6 , cd^7L , cd^8L^2 , cd^9L^3 , and $cd^{10}L^4$ states where c denotes a hole of the Fe 2p core level. The Coulomb interaction Q between the Fe 2p hole and the Fe 3d electron is expressed as Q which is fixed at $U/0.8$. With $\Delta = 2.0$ eV, $U = 3.5$ eV, and $(pd\sigma) = -1.2$ eV, the calculated spectrum can reproduce the Fe 2p XPS result as indicated by the solid curve in Fig. 3. Δ is smaller than U , indicating that CsFe₂Se₃ is a Mott insulator of charge-transfer type instead of Mott-Hubbard type.

The valence-band XPS spectra of BaFe₂Se₃, BaFe₂S₃, and CsFe₂Se₃ taken at 300 K are displayed in Fig. 4(a) and are compared with those of superconducting and

non-superconducting $K_xFe_{2-y}Se_2$. [6] Besides the shallow core levels such as Ba 5*p*, Cs 5*p*, and K 3*p*, the valence-band structures of the five systems are similar to one another. The spectral weight near the Fermi level increases in going from $CsFe_2Se_3$ to $BaFe_2Se_3$ to $BaFe_2S_3$, consistent with their transport properties. [8, 10, 11, 16]

Figure 4(b) shows the UPS spectra of $BaFe_2Se_3$, $BaFe_2S_3$, and $CsFe_2Se_3$ taken at 300 K. $BaFe_2S_3$ with the highest conductivity shows the tail of the spectral weight up to the Fermi level while $BaFe_2Se_3$ has the finite band gap of ~ 0.2 eV. The magnitude of the band gap observed in $BaFe_2Se_3$ is more or less consistent with the activation energies obtained from temperature dependence of resistivity by Lei *et al.* [8] $CsFe_2Se_3$ exhibits the largest band gap of ~ 0.8 eV consistent with the charge-transfer-type Mott insulator deduced from the Fe 2*p* XPS result.

The apparently homogeneous Fe valence and the relatively large band gap in $CsFe_2Se_3$ can be explained based on the idea of ligand hole. The smallness of the charge-transfer energy for the Fe^{2+} state indicates that, if Fe^{3+} exists in $CsFe_2Se_3$, it should take the d^6L configuration instead of d^5 . In this ligand hole picture, the two-leg ladder in $CsFe_2Se_3$ accommodates the d^6 -like and d^6L -like sites. Assuming that the d^6 -like and d^6L -like sites are aligned along the rung, the Se 4*p* hole should be located at the Se sites sandwiched by the two legs. This situation is schematically shown in Fig. 5 where all the Fe sites take the high-spin Fe^{2+} configuration and the S 4*p* holes are localized at the Se sites on the rungs. In this scenario, the Se 4*p* holes and the Fe 3*d* electrons are partially delocalized in $BaFe_2Se_3$ and $BaFe_2S_3$ and may cause the lattice (and magnetic) instability. In the low-temperature phase with the lattice distortion and the block-type magnetic order, the Se 4*p* holes and the Fe 3*d* electrons would be localized in the antiferromagnetic dimer with the Fe^{2+} high-spin configuration, and they are rather “itinerant” in the ferromagnetic dimer. Here, the Se 4*p* holes and the Fe 3*d* electrons in the ferromagnetic dimer are “itinerant” in a sense that they occupy a kind of molecular orbitals.

IV. CONCLUSION

In conclusion, we have studied the electronic structures of $BaFe_2X_3$ ($X = S$ and Se) and $CsFe_2Se_3$ using photoe-

mission spectroscopy. The Fe 2*p* core-level peaks consist of the two components in $BaFe_2X_3$, indicating that the itinerant and localized Fe 3*d* electrons coexist. The Fe 2*p* and valence-band spectra suggest that the itinerant Fe 3*d* electrons are more strongly confined in $BaFe_2Se_3$ than in $BaFe_2S_3$. On the other hand, the Fe 2*p* core-level peak of $CsFe_2Se_3$ exhibit the single component accompanied with the charge-transfer satellite. The insulating ground state of $CsFe_2Se_3$ can be viewed as a charge-transfer-type Mott insulator with localized Se 4*p* holes. In $BaFe_2X_3$ ($X = S$ and Se), the Se 4*p* or S 3*p* holes are partially delocalized and may cause the coexistence of the itinerant

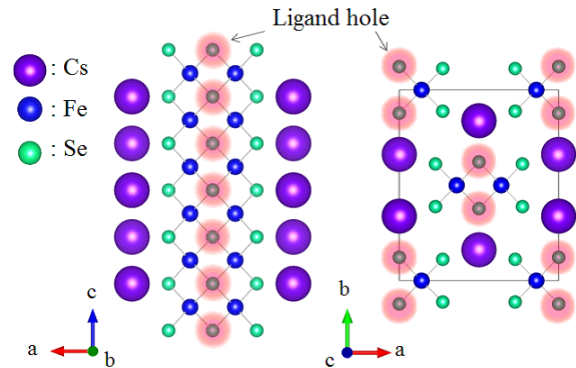


FIG. 5: Crystal structure and possible Se 4*p* hole distribution for $CsFe_2Se_3$ visualized using the software package Vesta[18].

and localized Fe 3*d* electrons. In future, the relationship between the chalcogen *p* holes, the lattice distortions, and the magnetic interactions should be further studied using various experimental and theoretical approaches.

Acknowledgements

The authors would like to thank Profs. H. Takahashi, H. Okamura, and Y. Uwatoko for valuable discussions. This work was partially supported by Grants-in-Aid from the Japan Society of the Promotion of Science (JSPS) (Grant No: 25400356). D.O. acknowledges supports from the JSPS Research Fellowship for Young Scientists.

-
- [1] J. Guo, S. Jin, G. Wang, S. Wang, K. Zhu, T. Zhou, M. He, and X. Chen, Phys. Rev. B **82**, 180520 (2010).
 - [2] Z. Shermadini, A. Krzton-Maziopa, M. Bendele, R. Khasanov, H. Luetkens, K. Conder, E. Pomjakushina, S. Weyeneth, V. Pomjakushin, O. Bossen, and A. Amato, Phys. Rev. Lett. **106**, 117602 (2011).
 - [3] F. Ye, S. Chi, W. Bao, X. F. Wang, J. J. Ying, X. H. Chen, H. D. Wang, C. H. Dong, and M. Fang, Phys. Rev. Lett. **107**, 137003 (2011).
 - [4] A. Ricci, N. Poccia, G. Campi, B. Joseph, G. Arrighetti, L. Barba, M. Reynolds, M. Burghammer, H. Takeya, Y. Mizuguchi, Y. Takano, M. Colapietro, N. L. Saini, and A. Bianconi, Phys. Rev. B **84**, 060511 (2011).
 - [5] M. Bendele, A. Barinov, B. Joseph, D. Innocenti, A. Iadecola, A. Bianconi, H. Takeya, Y. Mizuguchi, Y. Takano, T. Noji, T. Hatakeda, Y. Koike, M. Horio, A. Fujimori, D. Ootsuki, T. Mizokawa, and N. L. Saini, Sci. Rep. **4**, 5592 (2014).

- [6] M. Oiwake, D. Ootsuki, T. Noji, T. Hatakeda, Y. Koike, M. Horio, A. Fujimori, N. L. Saini, and T. Mizokawa, *Phys. Rev. B* **88**, 224517 (2013).
- [7] J. M. Caron, J. R. Neilson, D. C. Miller, A. Llobet, and T. M. McQueen, *Phys. Rev. B* **84**, 180409 (2011).
- [8] H. Lei, H. Ryu, A. I. Frenkel, and C. Petrovic, *Phys. Rev. B* **84**, 214511 (2011).
- [9] A. Krzton-Maziopa, E. Pomjakushina, V. Pomjakushin, D. Sheptyakov, D. Chernyshov, V. Svitlyk, and K. Conder, *J. Phys.: Condens. Matter* **23**, 402201 (2011).
- [10] J. M. Caron, J. R. Neilson, D. C. Miller, K. Arpino, A. Llobet, and T. M. McQueen, *Phys. Rev. B* **85**, 180405 (2012).
- [11] Y. Nambu, K. Ohgushi, S. Suzuki, F. Du, M. Avdeev, Y. Uwatoko, K. Munakata, H. Fukazawa, S. Chi, Y. Ueda, and T. J. Sato, *Phys. Rev. B* **85**, 064413(2012).
- [12] C. Monney, A. Uldry, K. J. Zhou, A. Krzton-Maziopa, E. Pomjakushina, V. N. Strocov, B. Delley, and T. Schmitt, *Phys. Rev. B* **88**, 165103 (2013).
- [13] Q. Luo, A. Nicholson, J. Rincón, S. Liang, J. Riera, G. Alvarez, L. Wang, W. Ku, G. D. Samolyuk, A. Moreo, and E. Dagotto, *Phys. Rev. B* **87**, 024404 (2013).
- [14] S. Dong, J.-M. Liu, and E. Dagotto, *Phys. Rev. Lett.* **113**, 187204 (2014).
- [15] M. V. Medvedev, I. A. Nekrasov, and M. V. Sadovskii, *JETP Lett.* **95**, 33 (2012).
- [16] F. Du, K. Ohgushi, Y. Nambu, T. Kawakami, M. Avdeev, Y. Hirata, Y. Watanabe, T. J. Sato, and Y. Ueda, *Phys. Rev. B* **85**, 214436 (2012).
- [17] N. L. Saini, Y. Wakisaka, B. Joseph, A. Iadecola, S. Dalela, P. Srivastava, E. Magnano, M. Malvestuto, Y. Mizuguchi, Y. Takano, T. Mizokawa, and K. B. Garg, *Phys. Rev. B* **83**, 052502 (2011).
- [18] K. Homma and F. Izumi, *J. Appl. Crystallogr.* **44**, 1272 (2011).